Journal of Electroceramics, 14, 45–52, 2005

Microstructural Analysis of X7R-Type $BaTiO_3$ Multilayer Ceramic Capacitors (MLCCs)

QIQUAN FENG & CASPAR J. McCONVILLE
The New York State College of Ceramics at Alfred University, Alfred, NY 14802, USA

Submitted March 11, 2004; Revised April 6, 2004; Accepted April 30, 2004

Abstract. The microstructures of typical commercial X7R MLCCs were characterized by transmission electron microscopy (TEM), using tripod polished specimens and ion milled samples. Core-shell structures were clearly observed in the TEM specimens, and glass phases located at the grain boundaries and triple points were frequently observed. Their chemical composition was analyzed using energy dispersive X-ray spectrometry (EDS), which showed bismuth ions diffused into the shell regions, while the cores were pure $BaTiO_3$. X-ray diffraction (XRD) suggested that the predominant phase in the microstructure had pseudocubic global symmetry, while ferroelectric domains were observed in TEM bright field (BF) images. The internal electrodes in the devices were an alloy of Ag/Pd, and these regions were found to have twinned crystal structures. The stress states in the interfaces between the electrodes and the dielectric layers were revealed, and no silver migration in the flux at the electrode-dielectric interfaces was observed.

Keywords: tripod polishing, core-shell structures, barium titanate, TEM, stress, microstructure

Introduction

Multilayer ceramic capacitors (MLCCs) are important electric components which are used in almost all areas of electronics. Their high volumetric capacitance and strong heat cycle shock resistance consistently outperform those of electrolytic capacitors as surface mounting devices (SMDs). For these reasons, MLCCs are expected to eventually replace electrolytic capacitors [1].

High-performance MLCCs are required to possess high volume efficiency and low manufacturing costs [2]. The keys to achieving these objectives are to reduce the thickness of the metal electrode and dielectric layers, to develop high permittivity dielectric materials and to utilize inexpensive internal electrodes and terminals [2–4].

However, challenges exist for all these research efforts to develop the high-performance MLCCs with low manufacturing costs. Conventionally, $BaTiO_3$-based dielectrics have been used in MLCCs, and in order to produce thinner dielectric active layers the average grain size of the $BaTiO_3$ must be reduced. The dielectric constant of $BaTiO_3$ is dependent on the grain size of the material [2, 5–8]. Moreover, electrode migration into the dielectric layers, which can affect the stability and dielectric properties of MLCCs, has to be considered as this is more likely to occur in systems with thinner active dielectric layers.

The production of capacitors with electrodes made of base metals such as nickel or copper requires a reducing atmosphere to protect those metals from oxidization when fired. Oxygen vacancies left behind in the dielectrics by this firing atmosphere lower the insulation resistance of the devices and degrade their reliability [3, 4, 9–13].

In order to meet the X7R industry standard [14], the dielectric permittivity with temperature properties of $BaTiO_3$ must be purposely modified by the addition of dopants including chemical shifters, pinchers, and depressors. Temperature-stable dielectric behavior can be achieved by chemical substitution in the ceramic material, by a small-grained microstructure or by the presence of 'core-shell' grains [15–19].

A characteristic of some X7R-type materials is the presence of core-shell structures within individual grains, where the cores are composed of pure barium titanate while the shells consist of barium titanate doped with additives, which may be Zr^{4+}, Ce^{4+}, Nb^{5+} or Bi^{3+}, amongst others [17–20]. It is widely accepted that the presence of core-shell structures in ceramics is attributed to chemical inhomogeneity [15–20]. Armstrong and Buchanan [21] used convergent beam electron diffraction (CBED) in the transmission electron microscope (TEM) to determine that both the core and shell in zirconia-modified barium titanate were tetragonal phases at room temperature. However, cubic shell phases have also been reported by other researchers in barium titanate systems doped with other additives [19].

Since the microstructure has a decisive influence on the electrical properties and reliability of the MLCCs [13, 22, 23], a deliberate design of the microstructure for individual grains is essential for the production of MLCCs with very thin dielectric layers and base-metal electrodes.

The objectives of the present work were to characterize the microstructural features of commercial X7R-type barium titanate MLCCs using TEM, to understand the interrelationships of the microstructural features observed, and make suggestions for future research with the aim of optimizing the microstructures through control of composition and processing conditions.

Experimental Procedure

The materials used for this study were commercial X7R-type MLCCs, supplied by Ferro Co., Penn Yan, NY. These devices are made using tape-casting techniques from $BaTiO_3$ which functions as the dielectric, and Ag/Pd layers which function as electrodes. The X7R-type MLCCs were fired in air at 850°C for 2 hours.

Specimens for TEM analysis were made using conventional techniques as well as using tripod polishing. The specimens were mechanically ground to ≈40 μm, then Ar-ion milled to electron transparency using a Dual Ion Beam Mill (Gatan 600). The specimens for scanning electron microscopy (SEM) and reflected optical microscopy (ROM) were made using tripod polishing procedures without etching. The introduction and development of tripod polishing procedures of TEM sample preparation for interfacial research have been reported elsewhere [24–26]. Powder samples made by grinding whole MLCCs (including both electrode and dielectric materials) to less than 10 μm were used for X-ray diffraction analysis.

The microstructures of the specimens (without carbon coating) were studied using a Jeol JEM-2000FX TEM (Jeol, Japan) operated at 200 kV. Phase identification was performed by selected area diffraction (SAD), and chemical information was obtained in the TEM, using a Princeton Gamma-Tech digital spectrometer and a PGT System4 Plus computer system (PGT, NJ). The structures of the capacitors were

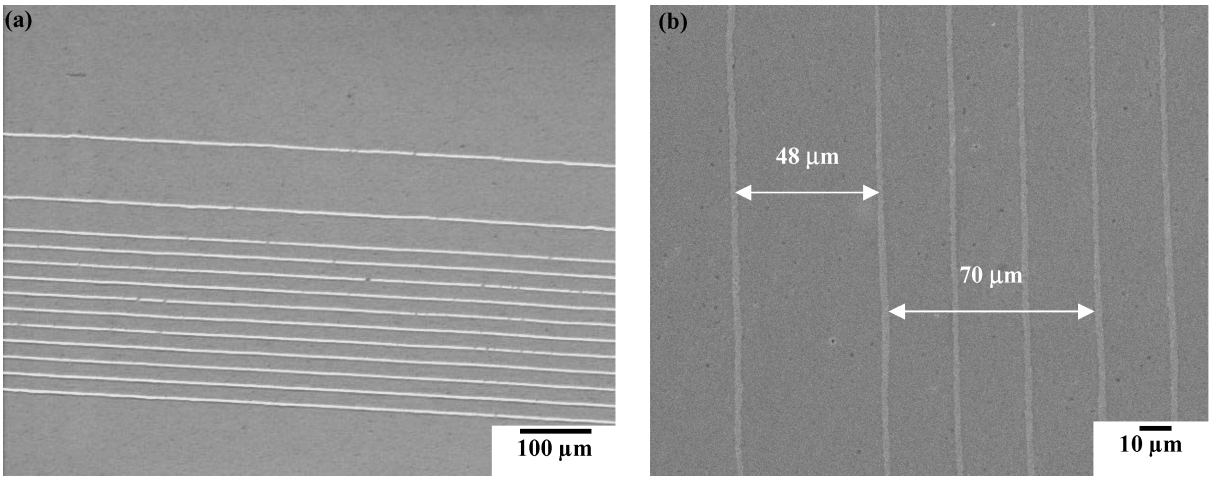

Fig. 1. (a) ROM and (b) SEM secondary electron (SE) image of the typical structure of MLCCs. The specimens were made using tripod-polishing.

observed using a Philips 515 SEM (FEI, Netherlands) and optical microscope (Reichert-Jung Polyvar-Met). X-ray diffraction (XRD) patterns were obtained using a XRG-3100 (PANalytical, Netherlands) using Cu Kα radiation ($\lambda = 1.54$ Å) with step size 0.02°.

Results and Discussion

MLCCs are manufactured by integrating dielectric layers separated by electrically conductive electrode layers, as shown by optical and scanning electron

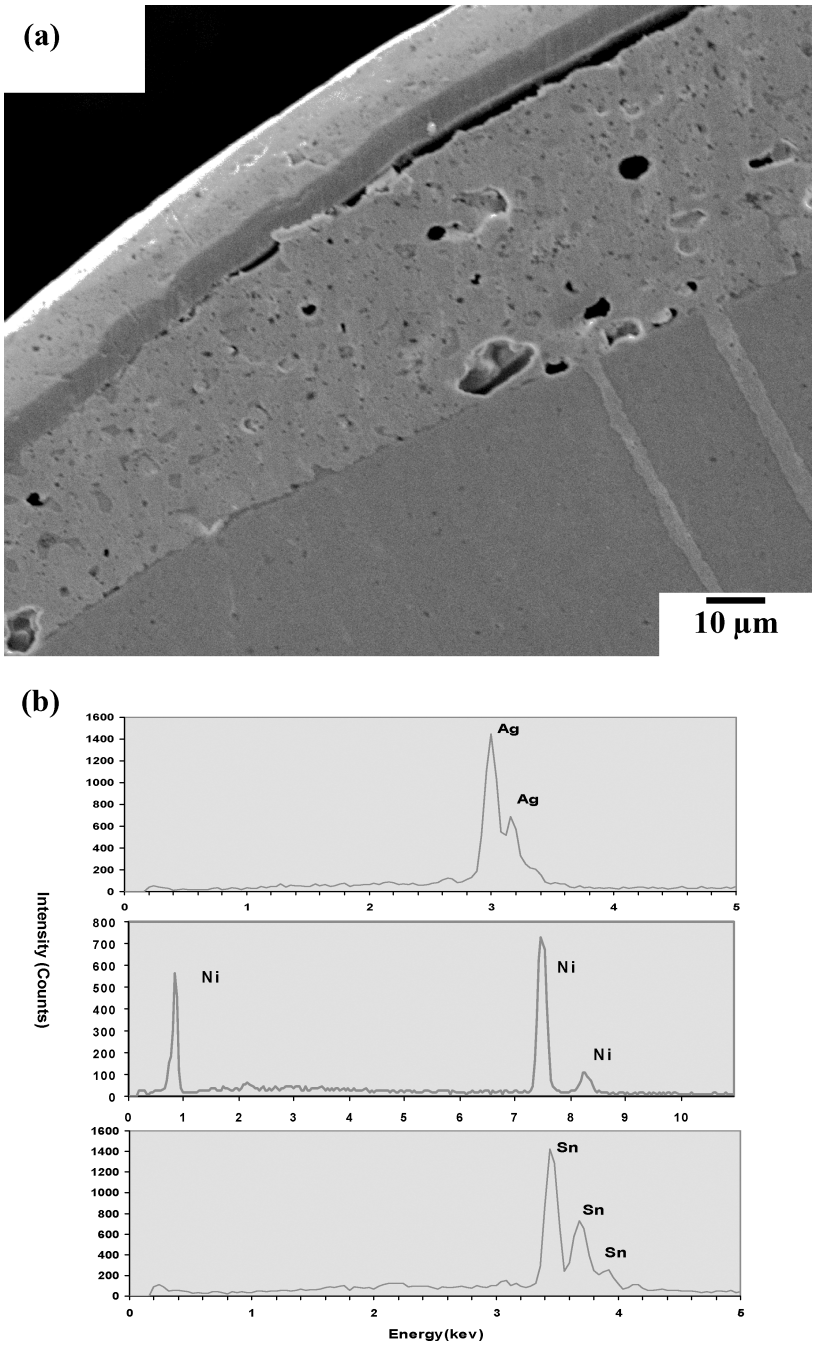

Fig. 2. (a) SEM SE image showing the terminals of MLCCs and (b) EDS analysis of the terminals.

microscopy (Fig. 1). The device shown has twelve active dielectric layers, and thirteen electrode layers with thicknesses of about 2 μm. Each active dielectric layer has a thickness of about 22 μm, except the first layer which is 90 μm and the second layer whose thickness is 48 μm. This design was used to achieve a particular capacitance value for the finished device.

The two opposing sets of electrodes in the capacitor are electrically connected at the end of the device by the terminals. Figure 2(a) clearly shows that the terminals have three different layers. The chemical composition of each terminal layer is shown in Fig. 2(b). Typically, the terminals are formed by dipping the MLCC into a thick film cement paste, usually composed of either Ag or Ag-Pd powder and glass frit, and sintering the device [27]. The first Ag layer is surrounded by a Ni layer, which is in turn covered by a Sn layer. The middle Ni layer works as a protective barrier to prevent silver migration, while the exterior Sn layer functions as a solderable layer and prevents oxidation of Ni [27]. The cracks visible in the interface between the Ni and Ag layers indicate that the bond between the two layers is weak. Figure 2(a) shows that the interfaces between the internal electrodes and the dielectric layers are clean, and no interdiffusion of the layers is visible. The dielectric layers appear dense, and the surface of the sample appears unscratched, owing to the tripod polishing method of sample preparation.

The microstructures of the dielectric grains were characterized by TEM. Figure 3 shows bright field (BF) images of typical dielectric regions. In these layers, the grain size has been deliberately optimized to be about 0.8 μm, corresponding to the maximum value of the dielectric constant. The center, or core part of the grains show ferroelectric domains, and these regions are surrounded by the featureless paraelectric areas called the shells. This microstructure, featuring coexistence of core and shell in one grain is called the 'core-shell' structure. The core-shell structure boundary as indicated by **A** in Fig. 3(a) is suggested to be coherent [16–18, 21]. The thickness of the domains varies between grains, but is generally less than 100 nm. Both the ribbon-like walls, a typical feature of 180° domains, and the stripe walls, characteristic of 90° domain walls, were observed in these materials. Some glass phases are seen to be located at the triple points (indicated by downward pointing arrows in Fig. 3(a)), and grain

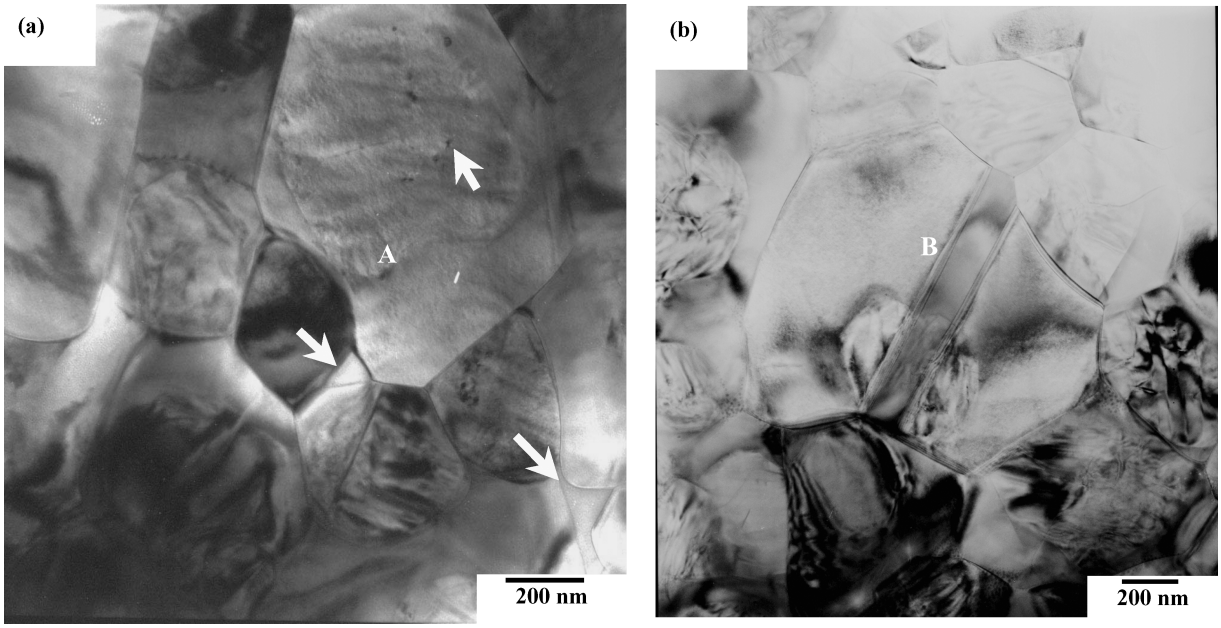

Fig. 3. Typical BF TEM images of X7R-type MLCCs showing morphologies of dielectric grains. Glass phases indicated with downward arrows and other second phases are indicated by an upward arrow in (a). Microstructures of MLCC show core-shell grains (**A**), and twinned crystals (**B**).

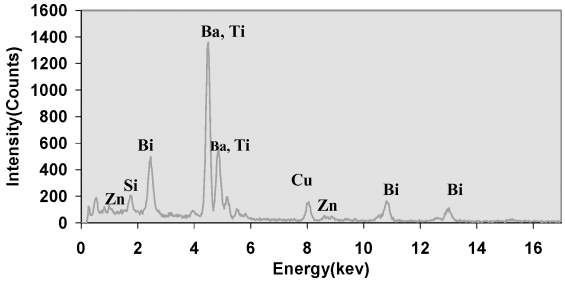

Fig. 4. Chemical composition of the glassy second phase analyzed by EDS.

boundaries. Some minor second phases (indicated in Fig. 3(a) by an upward arrow) were frequently observed in many grains in samples prepared by ion-milling. Further research showed they were artificial effects, as no such features were observed in tripod polished specimens. Large grains in the matrix show twin structures, as shown in Fig. 3(b). The twin boundary, marked as **B** in Fig. 3(b) crosses the core-shell structure boundary indicating that twinning exists in both the core and the shell. The twins in this material were found to be (111) twins.

The chemical composition of the glass phases analyzed by EDS were silicon, bismuth and zinc, as shown in Fig. 4. These are common dopants for X7R-type MLCCs fired at low temperatures. Bi_2O_3 and SiO_2 are glass formers while ZnO works as a glass network modifier. Liquid phase sintering is the main densification mechanism in the dielectric active layers. Although in some cases the glass fluxes formed continuous phases by crossing several dielectric and electrode layers, no electrode metal elements such as silver and palladium were observed in them. Moreover, no toxic elements such as Pb or rare earth elements like Ce were found. This makes the manufacturing environment much safer, and so helps to reduce the production costs. The glass phases, however, play a very important role in the microstructural development of the dielectric layers.

A representative BF image of the core-shell structure is shown in Fig. 5(a). The results of EDS point-by-point analysis to determine the chemical composition of the cores and the shells are shown in Fig. 5(b). As expected, the dopant ions were only found in the shell and were absent in the core regions. The concentration of bismuth changes dramatically at the interface between core and shell. The paraelectric phases of the shells were formed by diffuse phase transition, and similar phenomena have been reported in systems which used different dopants [15–20]. The inhomogeneous chemical composition between the core and shell indicates the core-shell structure is not a thermodynamically stable state. As a result, it is essential to design and control the sintering conditions accurately when manufacturing this type of MLCC. Clearly, the glass phases are the original source of the dopant ions which diffuse into the shell regions of the grains.

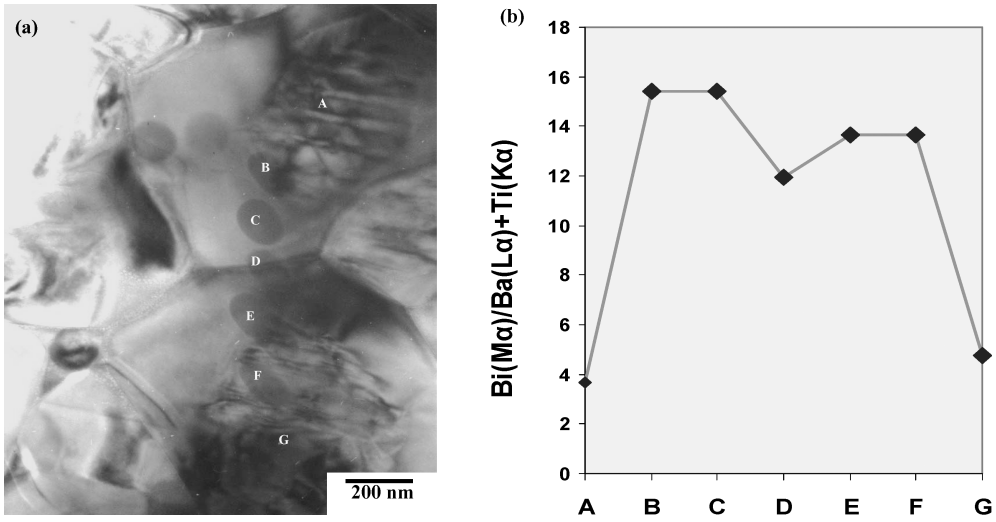

Fig. 5. (a) BF image showing core-shell structures and (b) corresponding chemical compositions of cores and shells analyzed by EDS. The relative concentration of bismuth is calculated as $Bi(M_\alpha)/[Ba(L_\alpha) + Ti(K_\alpha)]$.

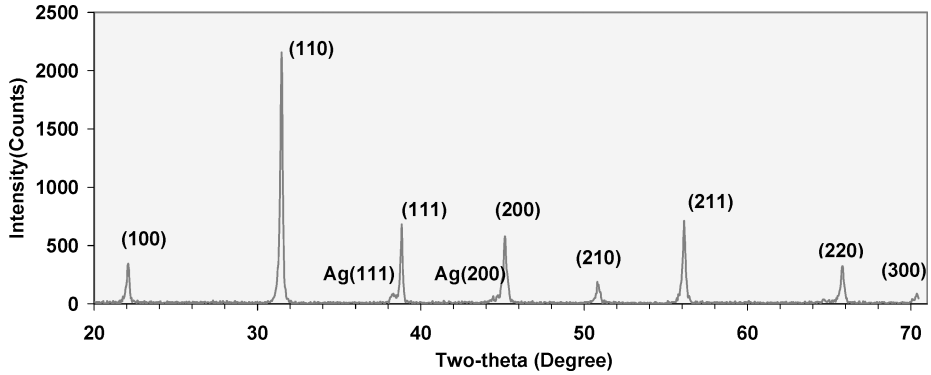

Fig. 6. Powder XRD of the MLCC materials.

As shown in Fig. 6, powder XRD patterns for the MLCC material indicate that the main crystal phases are cubic, despite the fact that ferroelectric domains, characteristic of the tetragonal phase, were observed in the core regions of the grains in BF TEM images (Fig. 5). The characteristic peak splitting of the (200) peak, which would indicate a tetragonal $BaTiO_3$ phase, is not seen in this XRD pattern. Based on this and TEM evidence, it is suggested that the lattice of the tetragonal core of the grain is distorted into a pseudocubic structure by stresses imposed by the paraelectric shell. The deviation of the *c*/*a* ratio from 1 is very small, and as such both phases appear cubic in XRD. The XRD results indicate that the cores of the $BaTiO_3$ grains remained deformed from the tetragonal to the pseudocubic structure even at room temperature. The probable explanation for this is the existence of complex stress states between the cores and shells in these grains. The XRD data, combined with the BF TEM images, suggest that the global symmetry of the materials (as opposed to the local symmetry) is pseudocubic at room temperature.

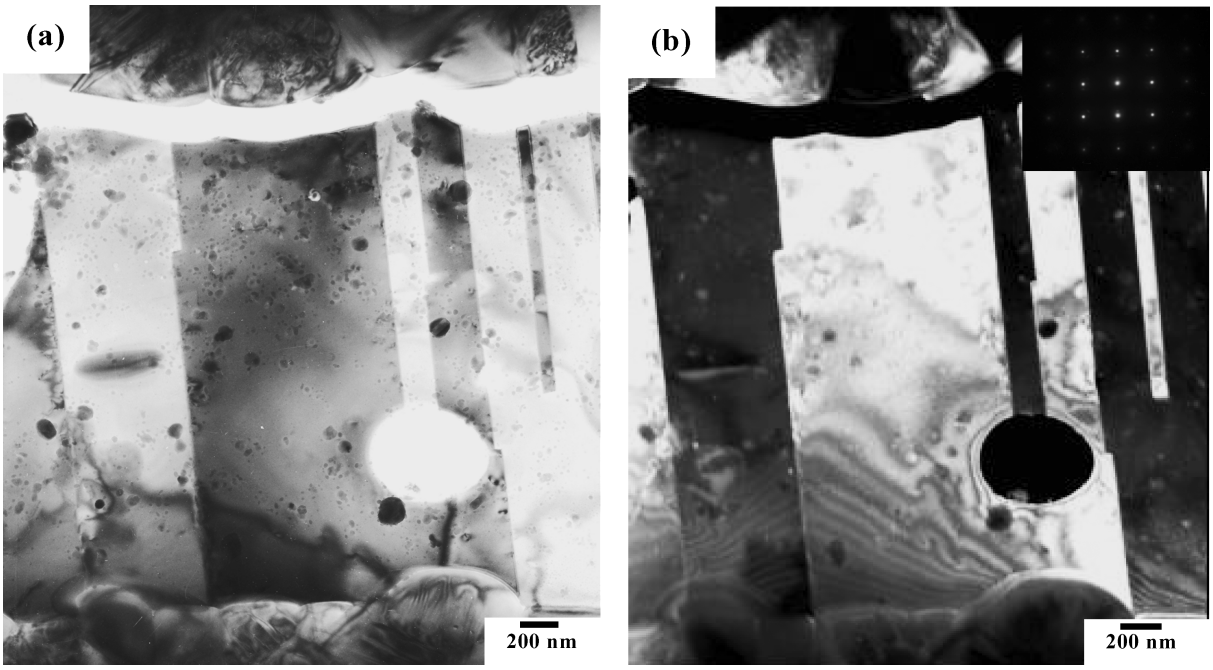

Fig. 7. (a) BF and (b) DF of internal electrode layer showing twinned crystals; Inset SAD pattern is a [100] zone axis.

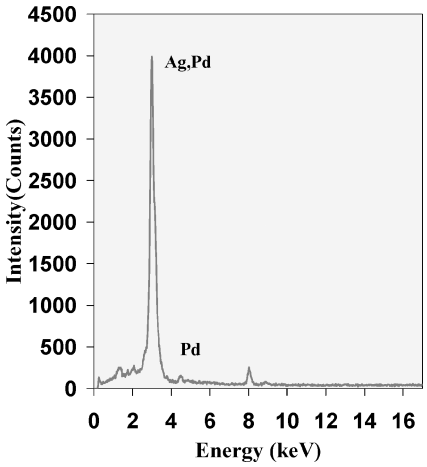

Fig. 8. The Ag/Pd internal electrode analyzed by EDS.

Figure 7 shows (a) BF and (b) dark-field (DF) images for a region of the internal electrode layer, showing the presence of twins in the microstructure. The chemical composition of the internal electrodes analyzed by EDS is silver and palladium, as shown in Fig. 8 (the copper peak visible at 8 keV is an artifact of sample preparation). Selected area diffraction of this phase is shown inset in Fig. 7(b) which shows it is a single, cubic phase. Clearly, silver and palladium have formed a continuous solid solution. The internal electrodes are twinned crystals, as shown in Fig. 7. The bend contours observed in the DF image (Fig. 7(b)) indicate that a stress state may exist between the electrodes and the dielectric layers. This stress probably arose from the mismatch of thermal expansion coefficients between the electrode and dielectric materials. In part, this stress is relieved by forming twinned crystals in the electrode layer.

The microstructure of heterogeneous interfaces between electrodes and dielectrics in cofired MLCCs is shown in Fig. 9(a). The electrode-dielectric interfaces could not be prepared for TEM analysis using ion-milling techniques, as the internal electrodes are preferentially removed by the milling process. However, TEM specimens with large areas of electron transparency across several dielectric layers integrated with electrodes can be obtained using tripod polishing procedures. Glass phases were observed at the

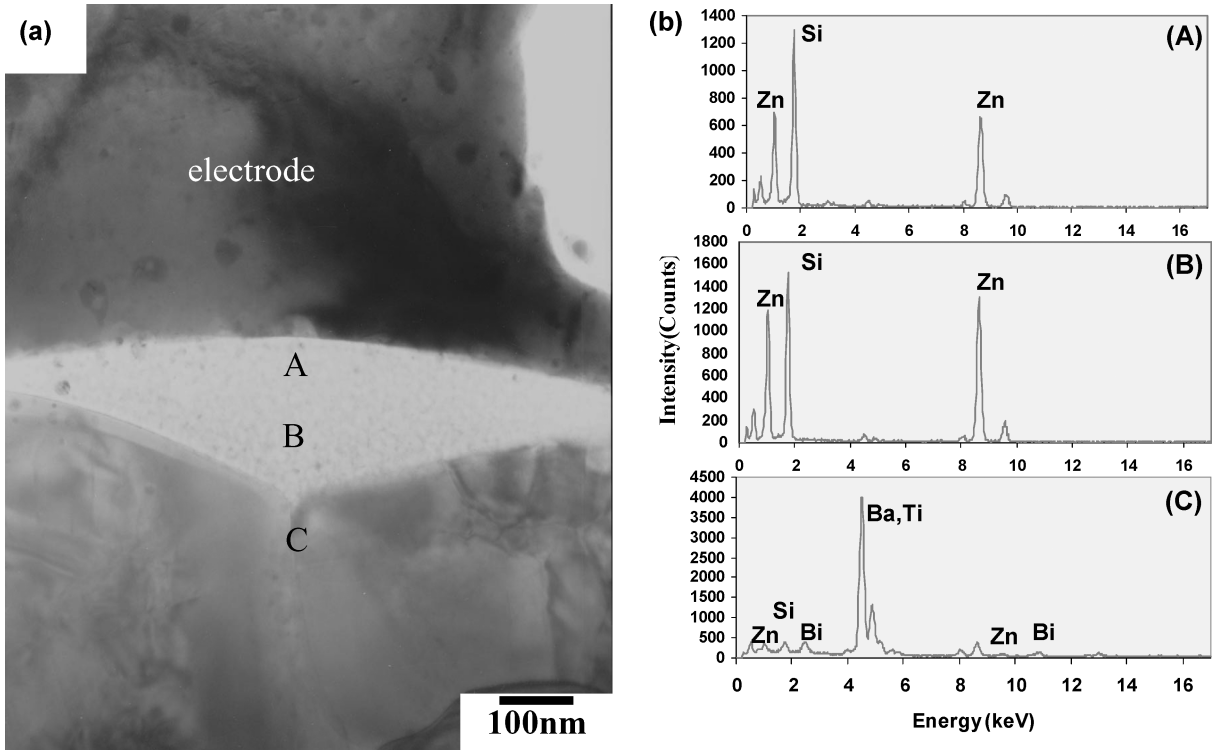

Fig. 9. (a) BF image of the electrode-dielectric interface; (b) EDS point-by-point analysis to show no silver migration in the flux.

electrode-dielectric interfaces, forming sandwich structures. EDS point-by-point analysis, shown in Fig. 9(b), did not show any silver migrated into the flux. The present work supports the assumption that silver diffusion into the dielectrics is negligible during the cofiring process [28].

Of the noble metals, silver has the lowest resistivity and is the most economical. Silver mixed with palladium to form a single phase solid solution will effectively decrease the migration of silver in the microstructure. Since noble metal electrodes were used in this type of MLCC, it can be deduced that the original materials were fired in an oxidizing atmosphere.

Conclusions

- The microstructures of commercial X7R-type MLCCs were studied by TEM, SEM and ROM using ion milled and tripod polished specimens. The termination has three layers: silver, nickel and tin, from inside to outside;
- Core-shell structures were predominant in the microstructure of the dielectric layers analyzed by TEM. Glass phases were frequently observed at the grain boundaries and triple points. The chemical composition of the glass phases analyzed by EDS was Zn, Bi, and Si. Both core and shell structures exhibited twins in some large grains.
- EDS point-by-point analysis showed that the shell regions contained dopant bismuth ions, while the cores were pure $BaTiO_3$. Bismuth was the only component of the glass phase observed which had diffused into the shell regions;
- The powder XRD pattern and BF TEM images indicated that the tetragonal structure of $BaTiO_3$ grains in this modified system were not very pronounced in the core, and that in the shell paraelectric phases were the norm. The high stress state existing in the core-shell structure is suggested from the BF TEM images and the powder XRD pattern obtained.
- Silver-palladium alloy is the internal electrode of this type of the MLCC. The stress arising from the mismatch of thermal expansion coefficients between the dielectric and electrode layers was observed. The internal electrodes show twinned structures. The electrode-dielectric interfaces have sandwich structures with the glass phase located between the electrode and dielectric layers. No silver migration into this flux was found.

References

1. T. Suzuki, M. Ueno, Y. Nishi, and M. Fujimoto, *J. Am. Ceram. Soc.*, **84**(1), 200 (2001).
2. S.F. Wang and G.O. Dayton, *J. Am. Ceram. Soc.*, **82**(10), 2677 (1999).
3. D.F.K. Hennings, *J. Euro. Ceram. Soc.*, **21**, 1637 (2001).
4. T.G. Reynolds III, *Am. Ceram. Soc. Bull.*, **80**(10), 29 (2001).
5. K. Uchino, E. Sadanaga, and T. Hirose, *J. Am. Ceram. Soc.*, **72**(8), 1555 (1989).
6. G. Arlt, D. Hennings, and G. de With, *J. Appl. Phys*. **58**(4), 1619 (1985).
7. W.R. Buessem, L.E. Cross, and A.K. Goswami, *J. Am. Ceram. Soc.*, **49**(1), 33 (1966).
8. M.H. Frey and D.A. Payne, *Phys. Rev. B*, **54**(5), 3158 (1966).
9. J.L. Paulsen and E.K. Reed, *Microelectr. Reliabi.* **42**(6), 815, (2002).
10. I. Burn and G.H. Maher, *J. Mater. Sci.*, **10**(4), 633 (1975).
11. D. Hennings and H. Schreinemacher, *J. Eur. Ceram. Soc.*, **15**(8), 795 (1995).
12. X.W. Zhang, Y.H. Han, M. Lal, and D.M. Smyth, *J. Am. Ceram. Soc.*, **70**(2), 100 (1987).
13. J. Rodel and G. Tomandl, *J. Mater. Sci.*, **19**(11), 3515 (1984).
14. Electronic Industries Association, Specification #RS198.
15. Y. Park and S.A. Song, *J. Mater. Sci: Materials in Electronics*, **6**, 380 (1995).
16. D. Hennings and G. Rosenstein, *J. Am. Ceram. Soc.*, **67**(4), 249 (1984).
17. H.Y. Lu, J.S. Bow, and W.H. Deng, *J. Am. Ceram. Soc.*, **73**(12), 3562 (1990).
18. S.H. Yoon, J.H. Lee, D.Y. Kim, and N.M. Hwang, *J. Am. Ceram. Soc.*, **85**(12), 3111 (2002).
19. S. Pathumarak, M. Al-Khafaji, and W.E. Lee, *British Ceramic Transactions*, **93**(3), 114 (1994).
20. F. Azough, R. Al-Saffar, and R. Freer, *J. Euro. Ceram. Soc.*, **18**, 751 (1998).
21. T.R. Armstrong and R.C. Buchanan, *J. Am. Ceram. Soc.*, **73**(5), 1268 (1990).
22. Y. Mizuno, T. Hagiwara, H. Chazono, and H. Kishi, *J. Euro. Ceram. Soc.*, **21**, 1649 (2001).
23. Y. Mizuno, Y. Okino, N. Hohzu, H. Chazono, and H. Kishi, *Jpn. J. Appl. Phys.*, **37**, 5227 (1998).
24. S.J. Klepeis, J.P. Benedict, and R.M. Anderson, in *Materials Research Society Symposium Proceedings*, edited by J.C. Bravman, R.M. Anderson, and M.L. McDonald (Materials Research Society, Pittsburgh, PA, 1988), Vol. 115, p. 179.
25. J.P. Benedict, R.M. Anderson, S.J. Klepeis, and M. Chaker, in *Materials Research Society Symposium Proceedings*, edited by R.M. Anderson (Materials Research Society, Pittsburgh, PA, 1990), Vol. 199, p. 189.
26. R. Anderson, S. Klepeis, and J. Benedict, South Bay Technology's Technical Library, Report Number 33.
27. H.V. Trinh and J.B. Talbot, *J. Am. Ceram. Soc.*, **86**(6), 905 (2003).
28. R.Z. Chen, X.H. Wang, Z.L Gui, and L.T. Li, *J. Am. Ceram. Soc.*, **86**(6), 1022 (2003).